

An Optimal Design Method of Hydrostatic Turntable Based on FPSO Algorithm

Yongsheng Zhao ✉ – Jiaqing Luo – Ying Li – Tao Zhang – Honglie Ma
Institute of Advanced Manufacturing and Intelligent Technology, Beijing University of Technology, China
✉ yszhao@bjut.edu.cn

Abstract *The load capacity of hydrostatic turntables is predominantly governed by the design of oil pads. Optimizing oil pad parameters can substantially enhance turntable performance while reducing power consumption. This study introduces a fuzzy particle swarm optimization (FPSO) algorithm that incorporates compression factors into the particle swarm optimization (PSO) framework to optimize the parameters of oil pads. Reduce its power consumption by about 40 %, while the error between experimental and theoretical values is only 8 %. Compared with traditional PSO algorithms, FPSO converges more reliably in multiparametric environments.*

Keywords *hydrostatic turntable, finite difference method, Reynolds equation, fuzzy particle swarm optimization algorithm, performance optimization*

Highlights

- *Introduced FPSO algorithm with compression factors for oil pad optimization.*
- *FPSO cut hydrostatic turntable power use by ~40%, boosting energy efficiency.*
- *FPSO showed strong convergence and 8% error, outperforming traditional PSO.*

1 INTRODUCTION

In heavy computer numerical control (CNC) machine tools, the hydrostatic turntable is a critical component that not only supports the machine tool but also provides high-precision movement. With advancements in hydrostatic bearing technology, its analysis and optimization have become increasingly complex, requiring extensive numerical calculations. Additionally, the size deviation of the oil pad significantly affects the oil film pressure distribution. Since millimeter-level precision control is essential for maintaining the high-precision rotation of the turntable, an efficient optimization algorithm is needed to optimize the load-carrying capacity of the circular oil pad. The particle swarm optimization (PSO) algorithm with a compressibility factor is an effective computational method, improving both the precision and convergence speed of the PSO algorithm.

The Reynolds equation is commonly used to evaluate hydrostatic turntables. It is a two-dimensional, second-order partial differential equation that incorporates parameters such as pressure, film thickness, and density. Several research teams have employed the Reynolds equation to analyze hydrostatic bearings and address engineering problems [1,2]. Wang et al. [3] numerically modified the classical Reynolds equation by considering the transient film thickness changes and surface deformation effects in the elastohydrodynamic lubrication (EHL) state. On this basis, Singh et al. [4] applied the improved Reynolds equation to analyze different oil pad configurations under hydrodynamic lubrication (HL) conditions and proved its adaptability under different lubrication systems. Gustafsson et al. [5] improved the Reynolds equation by incorporating the warm viscosity effect into the EHL model. Instead, Yang et al. [6] extended the equation with a non-Newtonian rheological model, which is commonly applied to the study of HL in complex fluids under steady-state conditions. Masjedi and Khonsari [7] proposed a numerical solution to the Reynolds equation by implementing the continuous successive over-relaxation (SOR) technique, which is particularly effective for solving transient EHL problems involving coupling pressure-deformation-film thickness interactions. El Khlifi et al. [8] extended the modeling framework by incorporating non-Newtonian fluid rheology and improved energy equations, a typical HL approach for solving steady-state viscous flows with complex fluid behavior. Li and Chen [9] derived an approximate expression for bearing surface roughness and obtained results by solving the Reynolds equation. Liu et al. [10] presented Reynolds expressions for bearings of various shapes, while Khakse et al. [11] formulated a Reynolds equation in spherical coordinates.

The PSO algorithm was initially proposed by Kennedy and Eberhart [12]. It is inspired by the predatory behavior of birds and fish, simulating their flight and foraging patterns to achieve optimal solutions through collective intelligence. This swarm intelligence-based optimization technique is simple to implement and has been applied to various fields, including bearing optimization. To ensure the convergence of the PSO algorithm, a compression factor is required [13]. Several studies [14-16] have attempted to improve the precision and convergence speed of the PSO algorithm by modifying parameter values. Niu et al. [17] developed a method for hyperstatic analysis and motion error prediction, validating its effectiveness but not optimizing it using an improved PSO algorithm. Chen and Li [18] introduced a novel multi-sensor signal analysis method for centrifugal pump fault diagnosis using an improved PSO algorithm, significantly enhancing structural optimization complexity and reducing computation time. Zhou et al. [19] proposed an improved PSO algorithm to reduce computational complexity, while Paikray et al. [20] applied an enhanced PSO algorithm to generate optimal, collision-free trajectories for robots in cluttered environments. Zhang et al. [21] improved the PSO algorithm by introducing dynamic inertia weights and gradient information, improving bearing fault diagnosis accuracy. Sana et al. [22] integrated an improved PSO algorithm with blockchain technology to enhance efficiency and security. Liu et al. [23] utilized an improved PSO algorithm to iteratively optimize the parameters of the gcForest model, achieving optimal diagnostic accuracy. Cheng et al. [24] applied different types of hydrostatic bearings to the PSO algorithm. Chang and Jeng [25] employed the

 DOI: 10.5545/sv-jme.2025.1366

PSO algorithm to design a double shim hydrostatic bearing. Srisha Rao and Jagadeesh [26] used vector-based evaluation to enhance the PSO algorithm convergence. Tang et al. [27] applied the PSO algorithm to workshop scheduling optimization, and Luo et al. [28] proposed a new group update method to improve species-based algorithms. Finally, Liu et al. [29] reviewed various optimization methods, highlighting the widespread application of the PSO algorithm across multiple domains.

In order to improve the load-bearing performance of the hydrostatic turntable and further reduce power consumption. This study modifies the Reynolds equation based on the working conditions of the hydrostatic turntable, and then uses the finite difference method (FDM) to solve the pressure distribution and oil flow parameters. The fuzzy particle swarm optimization (FPSO) algorithm is proposed for optimizing the key parameters of the turntable and further improving its load-bearing capacity. Compared with the PSO algorithm, power consumption is reduced by about 40 %, and the experimental and theoretical values have an error of only 8 %. The experimental results show that using the FPSO algorithm can obtain optimal solutions for various parameters of the turntable and minimize power consumption, providing an important reference for optimizing and evaluating the load-bearing performance of the hydrostatic turntable.

2 METHODS AND MATERIALS

2.1 Model of Hydrostatic Turntable and Oil Pad

As a key component of CNC machine tools, the hydrostatic turntable, plays an important role in the field of precision machining [30]. Its working principle is based on the hydrostatic pressure bearing theory, with a pressurized oil film as the core working medium. During operation, the external oil pump transfers the high-pressure oil to each oil chamber of the rotary table through the precision oil circuit, forming an oil film with bearing capacity between the rotary body and the base of the hydrostatic turntable. This oil film acts as a near-frictionless surface, supporting the weight of the rotary body and enabling smooth rotation [6].

The oil pad on the base is the core component that determines the bearing capacity of the hydrostatic turntable. After the high-pressure oil enters the oil pad, it is evenly distributed on the surface of the oil pad through the precise control of the throttling device to form a stable oil film with a certain stiffness. Several oil pads are strategically arranged on the base to carry the rotary body together. The classic hydrostatic turntable model is shown in Fig. 1, showing the main components of the turntable, including the base support system, the rotating execution unit, the hydrostatic bearing unit, the hydrostatic control system, and the auxiliary function module.

The oil pad consists of a circular stepped pad with concentric oil pockets, incorporating oil pockets and oil seals. The classic circular oil pad structure is shown in Fig. 1, where R_0 is the oil pad radius, R_1 is the oil pocket radius, and H_0 is the oil film thickness. Typical values of the outer diameter of the general circular oil pad R_0 are between 50 mm and 300 mm [31], while the inner diameter R_1 is usually kept between 20 mm and 150 mm [31]. As a key parameter, oil film thickness H_0 has a significant impact on the performance of the hydrostatic turntable, and its typical range is from 10 μm to 50 μm [32].

As the oil film thickness tends to zero, the bearing capacity becomes nearly infinite, increasing the likelihood of oil film collapse and compromising the machine tool's safety. Thus, it is necessary to regulate oil film thickness within a safe range. The working conditions of the hydrostatic turntable are as follows [33]:

$$\begin{cases} H \geq H_0 \\ \sum_{i=1}^{N} W_i = mg \end{cases}. \tag{1}$$

2.2 Theoretical Model

In hydrostatic systems, the pressure distribution in the oil pad is described by the Reynolds equation. Before solving the Reynolds equation, the following dimensionless parameters must be defined:

$$\begin{gathered} \bar{p} = \frac{p}{p_0},\ \bar{p}_0 = 1,\ \bar{r} = \frac{r}{R_0},\ \bar{R}_0 = 1,\ \bar{z} = \frac{z}{H},\ \bar{h} = \frac{h}{H},\ \bar{H} = 1, \\ \bar{U}_r = \frac{U_r}{\frac{H_0^2 P_0}{R_0 \eta}},\ \ \bar{U}_\theta = \frac{U_\theta}{\frac{H_0^2 P_0}{R_0 \eta}},\ \ \bar{W} = \frac{W}{R_0^2 P_0},\ \ \bar{q} = \frac{Q}{\frac{H_0^3 P_0}{\eta}}, \end{gathered} \tag{2}$$

where p is the oil film pressure, P_0 is the oil pocket pressure, r is the radial coordinate, h is the oil film thickness, U_r is the radial velocity, U_θ is the circumferential velocity, W is the bearing performance, Q is the volume flow of the oil pad, η is the viscosity. Moreover $\bar{p}$ is the dimensionless pressure, $\bar{h}$ dimensionless oil film thickness, $\bar{U}_r$ dimensionless radial velocity, $\bar{U}_\theta$ dimensionless circumferential velocity, $\bar{W}$ dimensionless bearing performance, $\bar{q}$ dimensionless flow, z coordinate in the film thickness direction, and p_0 pocket pressure (reference pressure).

Circular oil pads are suitable for Reynolds equations in cylindrical coordinate form. The fan element is used to analyze the force of the

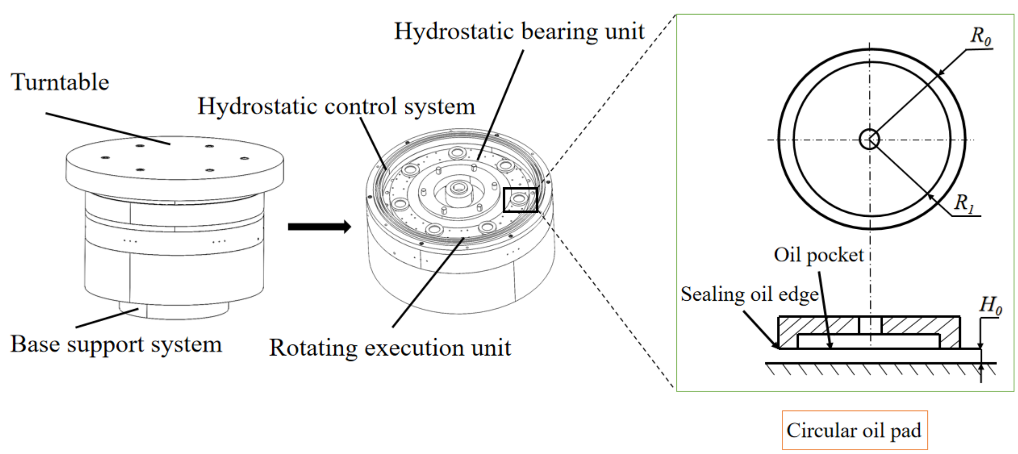

Fig. 1 Model of the hydrostatic turntable and circular oil pad

element, and the inertial force due to the centripetal acceleration of the element is introduced. The fan element forces used to analyze the circular oil pad are shown on Fig. 2. In polar coordinates, the Reynolds equation of the circular oil pad is [34]:

$$\frac{\partial}{\partial \bar{r}}\left(rh^{3}\frac{\partial \bar{p}}{\bar{r}}\right)+\frac{\partial}{\partial \bar{\vartheta}}\left(h^{3}\frac{\partial \bar{p}}{\bar{r}\bar{\vartheta}\bar{\vartheta}}\right)=0. \tag{3}$$

A common way to solve this partial differential equation is through FDM, which discretizes the equations into finite algebraic equations and iteratively solves them, as shown in Fig. 3. The Reynolds equation and its discretized form are expressed as follows [35]:

$$\begin{bmatrix} A1_{i,j} & A2_{i,j} & A3_{i,j} & A4_{i,j} & A5_{i,j} \end{bmatrix}\begin{bmatrix} \bar{p}_{i+1,j} \\ \bar{p}_{i-1,j} \\ \bar{p}_{i,j} \\ \bar{p}_{i,j-1} \\ \bar{p}_{i,j+1} \end{bmatrix}=0, \tag{4}$$

$$\begin{cases} A1_{i,j}=\dfrac{\bar{r}_i\bar{h}_{i,j}^{3}}{\bar{r}_{step}^{2}} \\ A2_{i,j}=\dfrac{\bar{r}_{i-1}\bar{h}_{i-1,j}^{3}}{\bar{r}_{step}^{2}} \\ A3_{i,j}=-\left(\dfrac{\bar{r}_i\bar{h}_{i,j}^{3}}{\bar{r}_{step}^{2}}+\dfrac{\bar{r}_{i-1}\bar{h}_{i-1,j}^{3}}{\bar{r}_{step}^{2}}+\dfrac{\bar{h}_{i,j-1}^{3}}{\bar{r}_i\,\bar{\theta}_{step}^{2}}+\dfrac{\bar{h}_{i,j}^{3}}{\bar{r}_i\,\bar{\theta}_{step}^{2}}\right) \\ A4_{i,j}=\dfrac{\bar{h}_{i,j-1}^{3}}{\bar{r}_i\,\bar{\theta}_{step}^{2}} \\ A5_{i,j}=\dfrac{\bar{h}_{i,j}^{3}}{\bar{r}_i\,\bar{\theta}_{step}^{2}} \end{cases}, \tag{5}$$

where [$A1$, $A2$,..., $A5$] is the coefficient vector and the pressure is assumed to be distributed across x_{pieces} nodes in the x direction and y_{pieces} nodes in the y direction. The value of the index i is an integer in [1,x_{pieces}], and the value of the index j is an integer in [1, y_{pieces}]. Therefore, Eq. (4) forms an algebraic system of equations of dimension $x_{pieces}\times y_{pieces}$, and its solution provides the numerical solution of the pressure distribution. Here, i and j represent the r and θ coordinates. $\bar{r}_{step}$ is the step size of the r coordinate, $\bar{\theta}_{step}$ is θ steps of coordinates. The boundary conditions for the pressure distribution are as follows: the pressure within the inner oil pocket is set to 1, while the pressure at the outer oil seal is 0 [36]:

$$\bar{p}_{i,j}=\begin{cases}1, & \bar{r}_i<\bar{R}_1 \\ 0, & \bar{r}_i=1\end{cases}. \tag{6}$$

The bearing capacity of the oil pad is determined using [25]:

$$\begin{cases} \bar{w}=\bar{p}\bar{r}d\bar{r}d\bar{\theta} \\ \bar{q}=\int\dfrac{\bar{z}^{2}-\bar{z}}{2\eta}\dfrac{\partial\bar{p}}{\partial\bar{r}}d\bar{z}, \quad \text{where} \quad \bar{r}_i=1 \end{cases}. \tag{7}$$

The parameters $\bar{w}$ and $\bar{q}$ are important indicators for evaluating the bearing capacity of the hydrostatic turntable. These parameters vary with changes in $\bar{R}_1$. Assuming that the delivery weight is constant, the pump power is expressed as follows [27]:

$$\begin{cases} P_0=\dfrac{mg}{N\bar{w}\pi R_0^{2}} \\ Q=\bar{q}\dfrac{H_0^{3}P_0}{\eta} \\ P_s=NP_0Q \end{cases}, \tag{8}$$

where P_s is the power consumption. During the optimization process, losses due to the electromechanical system's efficiency and pressure variations are neglected.

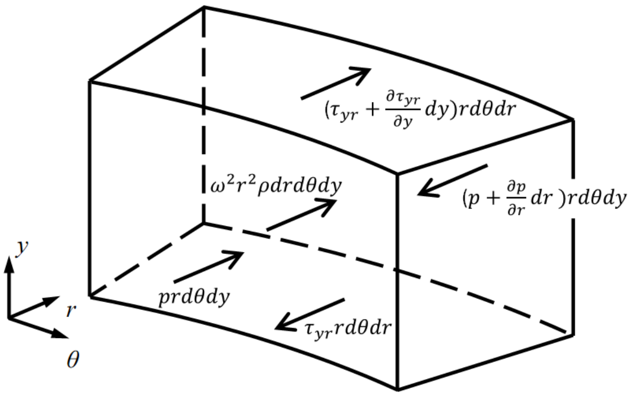

Fig. 2. Circular microelement forces in cylindrical coordinates

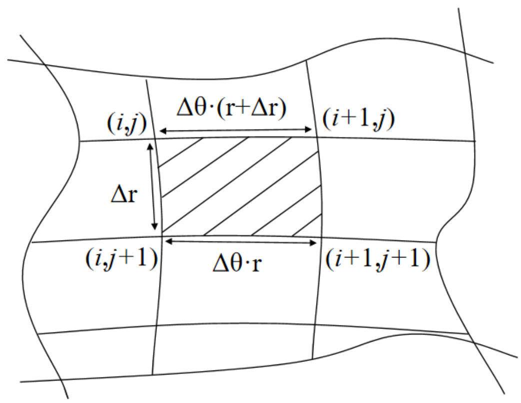

Fig. 3. Discretization of pressure

2.3 FPSO Algorithm

The PSO algorithm is a global search optimization method known for its simplicity and fast convergence. Due to its leapfrog nature, it efficiently locates the global optimum. This algorithm is particularly useful for optimizing problems involving multiple design variables and minimal parameters, where the number of particles is defined by N_p. Here, w is inertia weight, c_1 and c_2 are learning factors, X_i is particle position, V_i is search vector, P_i is individual optimal position, G_{best} is population optimal position, r_1 and r_2 are random numbers in the interval [0,1]. In Equation (9b), the first item is a memory term, representing the size and direction of the speed in the last iteration, the second item is a self-cognition term, and is referred to as the "self-cognition item" of particles. The third item is a group cognition term, indicating that the actions of particles are determined by their own experience and the best experience of their peers [18].

$$X_i^{n+1}=X_i^{n}+V_i^{n+1}, \tag{9a}$$

$$V_i^{n+1}=wV_i^{n}+c_1r_1\left(P_i^{n}-X_i^{n}\right)+c_2r_2\left(G_{best}^{n}-X_i^{n}\right). \tag{9b}$$

In cases with multiple local optima, the PSO algorithm may struggle to identify the global optimum. For instance, in Griewank function optimization, after initializing particles using the PSO algorithm, particles are easily attracted by local optima during iterations. This results in clustering around a local solution, which makes it difficult to find the optimal global solution due to reduced speed and limited information exchange. To address this limitation, a compression factor, also known as a constraint factor, can be introduced to control system convergence. This approach enables efficient exploration of different regions and improves solution quality. By increasing the compression factor, particle flight speed can be effectively controlled, thereby balancing local search capability and global convergence. This further enhances the global search capability and avoids the problem of premature convergence of the hydrostatic turntable in multi-objective parameter optimization. It has been verified by experiments that the best convergence accuracy and speed can be achieved when c_1 is 0.4 and c_2 is 0.9 [28]. This ensures the algorithm's accuracy and convergence speed. The modified equations incorporating the compression factor are given as follows [13]:

$$V_i^{n+1} = K \times \left(V_i^n + c_1 r_1 \left(P_i^n - X_i^n\right) + c_2 r_2 \left(G_{best}^n - X_i^n\right)\right), \tag{10a}$$

$$K = \left(\frac{(2)}{\left|2 - \varnothing - \sqrt{\varnothing^2 - 4\varnothing}\right|} \right), \quad \varnothing = c_1 + c_2 \text{ and } \varnothing > 4. \tag{10b}$$

Each individual in the PSO algorithm represents a value of R_1 so that $R_1 = X_n \cdot R_0$. The optimization objective is to minimize bearing losses. The termination condition for the optimization is defined as follows [25]:

$$\begin{cases} \left|x_n^{(k)} - x_n^{(k-1)}\right| \le tol_{PSO} \\ \max\left(x_n^{(k)}\right) - \min\left(x_n^{(k)}\right) \le tol_{PSO} \end{cases}. \tag{11}$$

3 RESULTS AND DISCUSSION

3.1 Theoretical Calculation

The algorithm of this research is shown in Fig. 4, which mainly includes three parts: first, using FDM to solve the Reynolds equation, and then evaluating the support force. Finally, the improved PSO algorithm with compression factor is used to solve the minimum power consumption problem of the oil pad.

The bearing capacity of the oil pad is analyzed using dimensionless bearing capacity and dimensionless flow parameters. The size of the oil pad influences both factors. Figure 5 presents experimental results demonstrating that the bearing capacity of the oil pad increases with the dimensionless size.

As shown in Fig. 6, increasing the dimensionless radius of the circular oil pad leads to an increase in both dimensionless bearing capacity and dimensionless flow rate. The dimensionless bearing capacity exhibits a linear increase with radius, while the dimensionless flow rate increases at a higher rate as the radius grows. This is because the increase in the dimensionless radius will expand the oil film pressure integral region, so that the bearing area is proportional to the square of the radius, thus significantly improving the hydrostatic bearing capacity. In addition, driven by the pressure difference, the effective path length of the oil flow along the radial direction is linearly related to the dimensionless radius, resulting in enhanced fluid energy transfer.

3.2 Experimental Verification

To verify the theoretical calculation, a 32-channel dynamic signal acquisition module is configured with an LMS modal test instrument. The installation gap was eliminated, and the repeatability of boundary conditions was ensured by the preloading method. An acceleration sensor was arranged on the turntable to monitor the vibration response, and the pressure distribution data was collected synchronously by the strain gauge attached to the surface of the oil pad. The experiments were carried out on the hydrostatic turntable of General Technology Group Tianjin First Machine Tool Corporation, China, as shown in Figs. 7a and b. The parameters of the hydrostatic turntable are presented in Table 1, while the size parameters of the tested circular oil pads are listed in Table 2.

Table 1. Relevant parameters of the hydrostatic turntable

Parameter	Value	Parameter	Value	Parameter	Value
R_0	0.075 m	n	20	tol_{FDM}	1×10^{-7}
m	25000 kg	η	0.08 Pa·s	tol_{PSO}	6

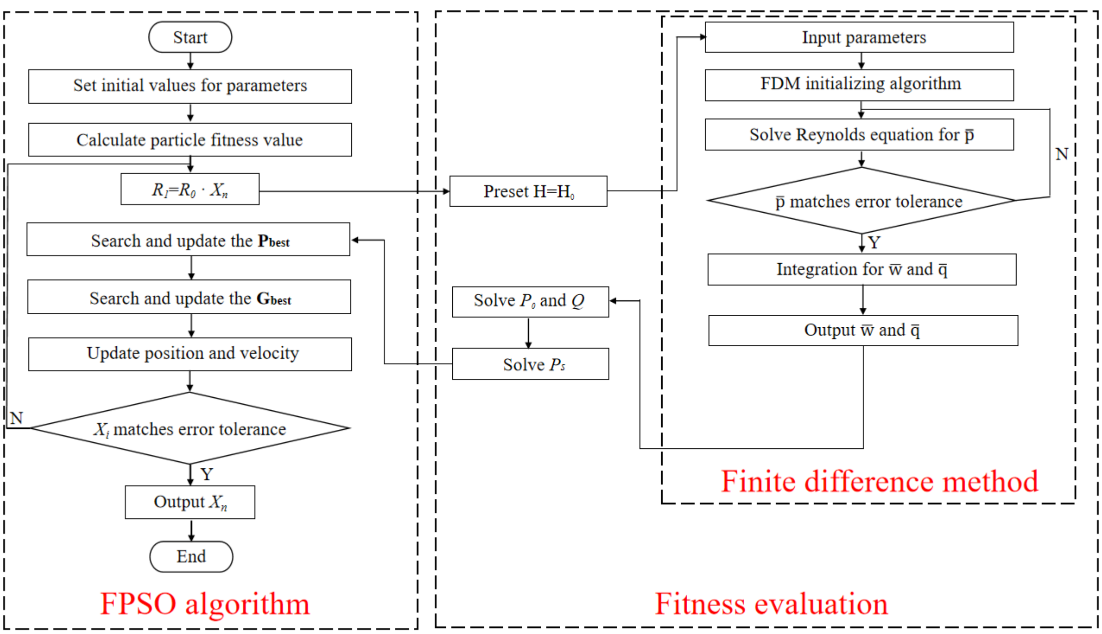

Fig. 4. Flowchart of the proposed algorithm

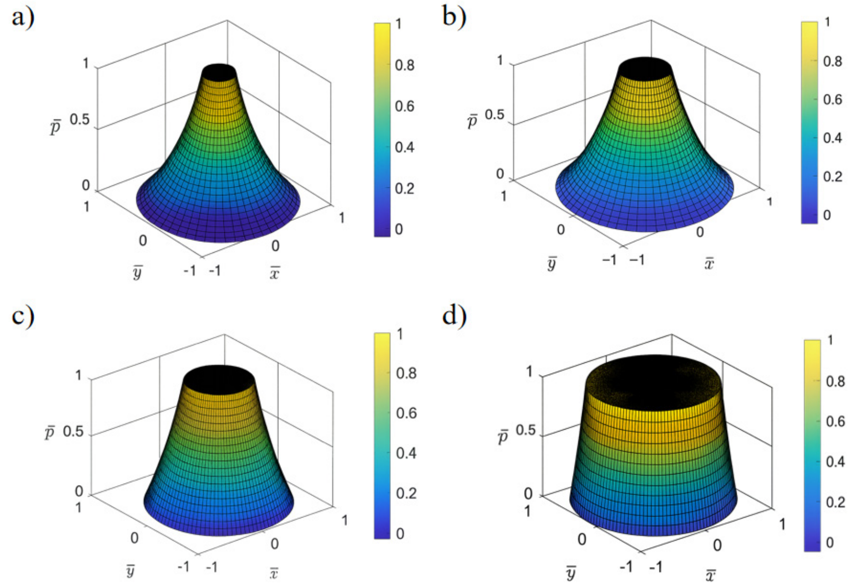

Fig. 5. Relationship between dimensionless pressure distribution and dimensionless oil pad radius: a) $\overline{R}_1$ = 0.2, b) $\overline{R}_1$ = 0.4, c) $\overline{R}_1$ = 0.6, and d) $\overline{R}_1$ = 0.8

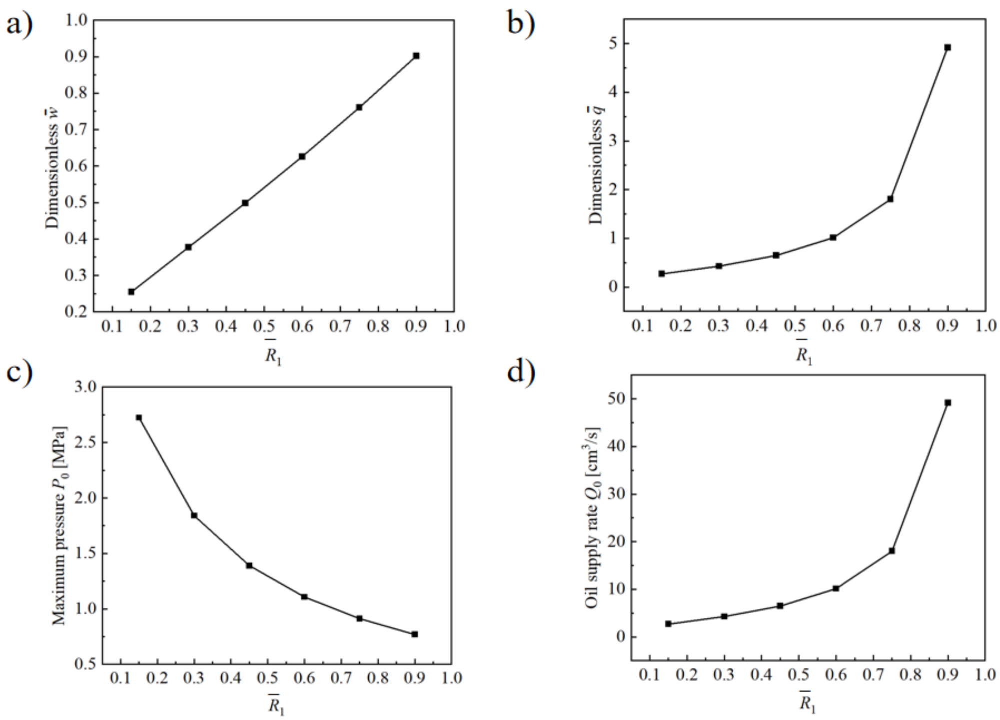

Fig. 6. Relationship between circular oil pad performance and pad size; a) dimensionless $\overline{w}$, b) dimensionless $\overline{q}$, c) maximum pressure P_0, and d) oil supply rate Q

Five circular oil pads of varying sizes were selected for testing. The test results are shown in Figs. 7c and d. Compared to theoretical calculations, the experimental values were lower, with a minimum error of approximately 8 %. The results indicate a certain deviation between theoretical and experimental values. The reason for the error is that the theoretical model usually ignores the nonlinear constitutive relationship of oil, the coupling effect of multiple physical fields, and the geometric deviation introduced by the manufacturing process, which leads to systematic error in the prediction of fluid mechanics behavior. In addition, experimental factors such as oil contamination and assembly errors further expand the error range. However, the trends of dimensionless bearing capacity and flow rate with respect to oil pad size remain consistent, confirming the feasibility of the theoretical calculations.

Table 2. Dimensional parameters of circular oil pads

	R_0 [m]	R_1 [m]	$\overline{R}$
Pad 1	0.033	0.01	0.3030303
Pad 2	0.033	0.015	0.4545454
Pad 3	0.033	0.02	0.6060606
Pad 4	0.033	0.025	0.7575758
Pad 5	0.033	0.028	0.8484848

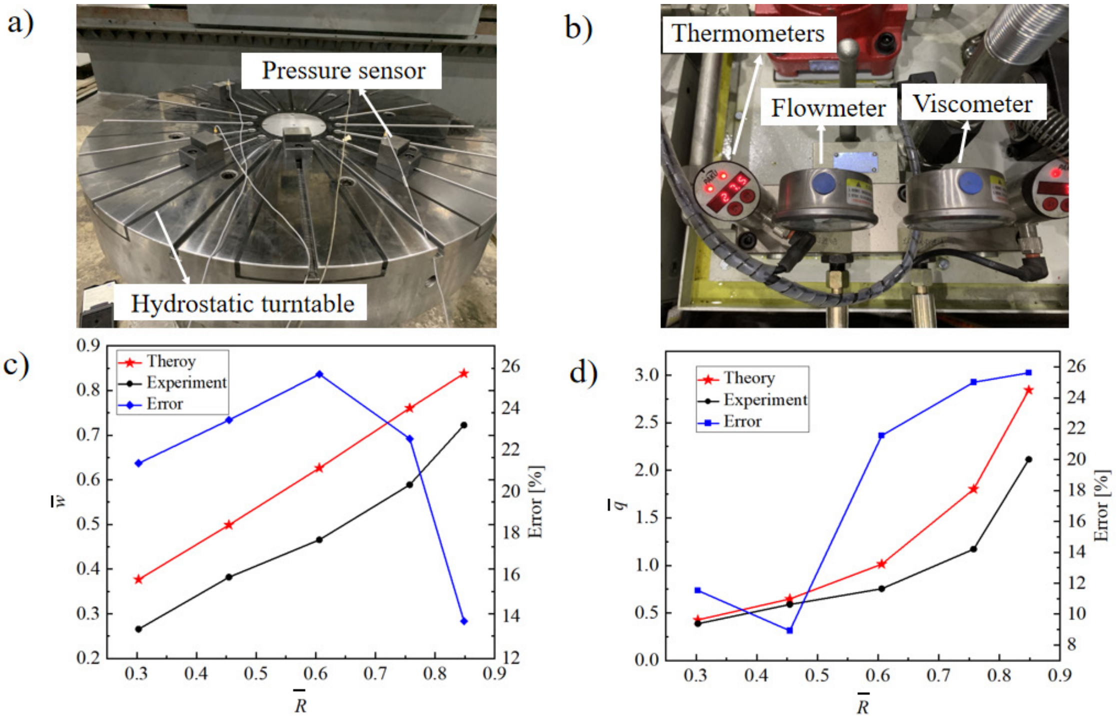

Fig. 7. Hydrostatic turntable testing and comparison of theoretical and experimental results; a) physical diagram of the hydrostatic turntable, b) data acquisition system, c) dimensionless bearing capacity, and d) dimensionless flow

3.3 Optimization of Various Parameters Based on FPSO Algorithm

The initial position and velocity of particle X_n within the defined domain were randomly assigned. The radius of the oil pad was assumed to be $R_1=X_n \cdot R_0$, linking its size to the particle positions. As the position of the particle in the search space changes, the X_n also changes, resulting in a corresponding change in the oil pad radius R_1. The film thickness was assumed to be H_0, and support performance was determined using the finite difference method to minimize power loss. The FPSO algorithm identified the global optimal solution by iteratively searching for the best fitness value, determining the optimal location, and power consumption. The effect of dynamic viscosity η, oil film thickness H_0, and the number of oil pads on pump power consumption was investigated. When the particle swarm size was set to five, convergence was achieved in seven cycles. The impact of η on pump power consumption is shown in Fig. 8, where η was set to 0.06, 0.08, and 0.1. The results indicate a negative correlation between η and pump power consumption. Variations in X_η and P_s remained minimal, suggesting that η has a limited effect on pump power consumption, increasing from 0.06 to 0.1 and reducing power consumption by only 20.6 W, with the optimal power consumption being 30.5 W when the P_s position is 0.549, and the optimal η is 0.1. The influence of oil film thickness H_0 on pump power was then examined. Under ideal conditions, the minimum oil film thickness can reach 5×10^{-5} m. To accommodate practical conditions, the minimum thickness was evaluated starting from 10×10^{-5}, as shown in Fig. 9. The results indicate a positive correlation between H_0 and pump power consumption. While H_0 had minimal influence on X_n, it significantly affected P_s. When the particle position reaches 0.565, the minimum power consumption is 407.6 W, and the optimal oil film thickness is 1×10^{-4} m. This shows that thicker films require higher support power. Finally, the effect of the number of oil pads on pump power was analyzed, as shown in Fig. 10. The number of oil pads was set to 10, 15, and 20, while other parameters remained constant.

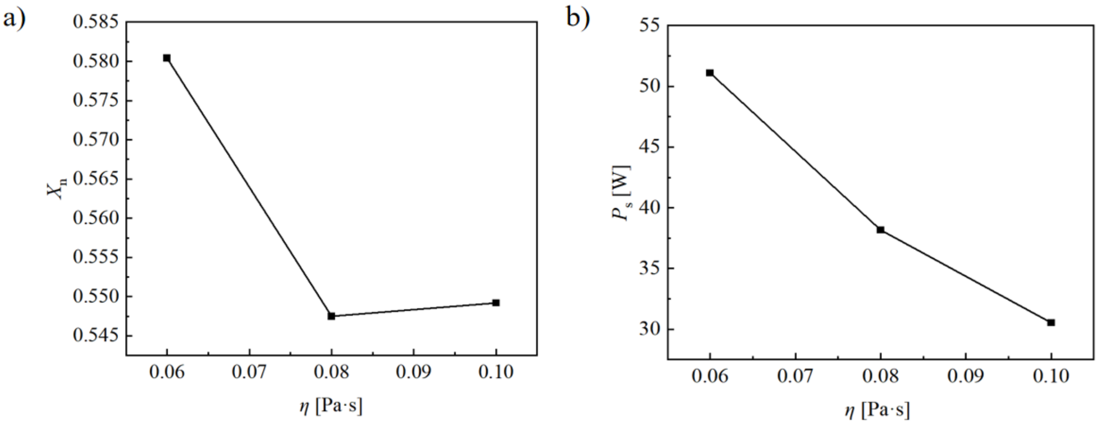

Fig. 8. The influence of different η on a) position of the particles, and b) power consumption

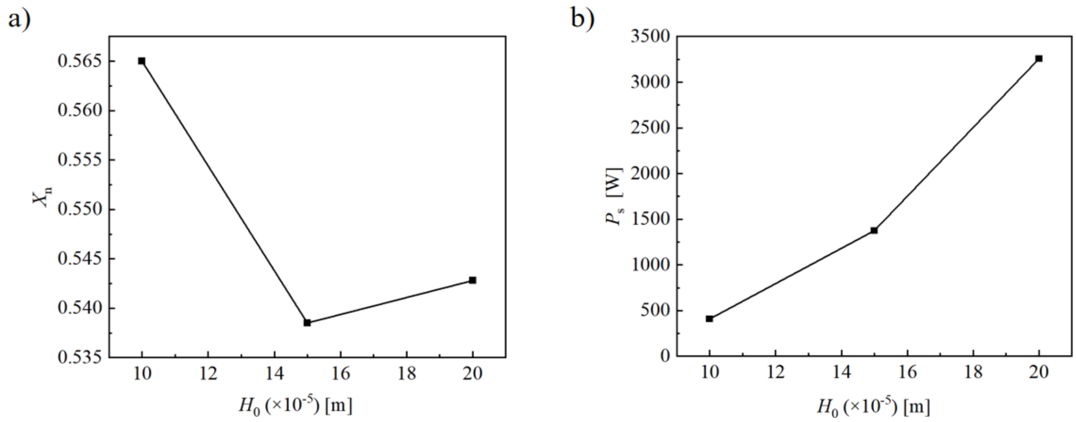

Fig. 9. The influence of different H_0 on; a) position of the particles in each iteration, and b) power consumption

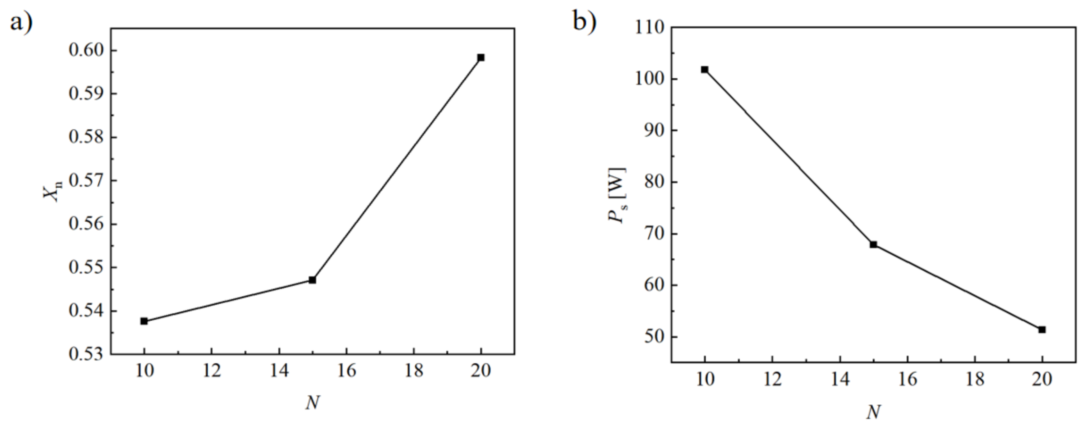

Fig. 10. The influence of different N on: a) position of the particles, and b) power consumption

The results indicate an inverse relationship between the number of oil pads and pump power consumption. When the particle position reaches 0.598, the optimal number of oil pads is 20, and the minimum power consumption is 51.3 W. Increasing the number of oil pads reduced overall power consumption. However, the number of oil pads had a relatively minor effect on power consumption compared to other factors. Overall, film thickness H_0 was identified as the primary factor affecting pump power consumption. Based on the experimental results and the operational constraints of the hydrostatic turntable, the optimal parameters were determined as $\eta=0.1$, $H_0=1\times10^{-4}$ m, and $N=20$. Under these conditions, the optimal power consumption of the turntable was $P_s=244.3$ W. By reducing the power consumption of the support, the hydraulic thermal load and the thermal drift caused by the increase in oil temperature and rotation axis are directly reduced, which is beneficial for the geometric accuracy and surface smoothness in heavy-duty CNC machining. Simultaneously, precise control of film thickness can achieve maximum energy-saving effect, while an appropriate number of oil pads can maintain load-bearing capacity and overturning stiffness. It also reduces operating costs, pump wear, and cooler load, and can reduce auxiliary cooling capacity.

4 CONCLUSIONS

To solve the optimization problem of load power consumption in a hydrostatic turntable, this study solved the Reynolds equation using the FDM method to analyze the bearing capacity of the hydrostatic turntable. The relationship between turntable parameters and power consumption was determined numerically. Based on these findings, an efficient optimization method for hydrostatic turntable design is proposed to solve the problem of premature convergence of traditional PSO in multivariable nonlinear optimization. The conclusions are as follows:

1. A FPSO algorithm has been proposed to address the shortcomings of single objective tuning and premature convergence in the design of multivariable parameters for hydrostatic turntables using the PSO algorithm. It improves the load-bearing performance while reducing power consumption.
2. Through FPSO algorithm optimization, the optimal parameters for the hydrostatic turntable can be obtained as follows: η = 0.1, $H_0=1\times10^{-4}$ m, $N=20$. The influence of various parameters on the bearing performance of the turntable has been clarified: $H_0>N>\eta$. The maximum energy-saving effect can be achieved by controlling the precise film thickness, while the appropriate number of pads can maintain load capacity and overturning stiffness.
3. The support power consumption of the pump has been reduced by about 40 %, and the theoretical calculation and experimental error is only 8 %. Further improving its load-bearing performance reduces thermal drift and operating costs in the turntable.

References

[4] Qiu, M., Bailey, B.N., Stoll, R., Raeymaekers, B. The accuracy of the compressible Reynolds equation for predicting the local pressure in gas-lubricated textured parallel slider bearings. *Tribol Int* 72 (2014) 83-89 **DOI:10.1016/j.triboint.2013.12.008**.

[5] de la Guerra Ochoa, E., Echávarri Otero, J., Sánches López, A., Chacón Tanarro, E. Film thickness predictions for line contact using a new Reynolds-Carreau equation. *Tribol Int* 82 133-141 (2015) **DOI:10.1016/j.triboint.2014.10.003**.

[6] Wang, N., Cha, K.-C., Huang, H.-C. Fast convergence of iterative computation for incompressible-fluid Reynolds equation. *J Tribol-T ASME* 134 024504 (2012) **DOI:10.1115/1.4006360**.

[7] Singh, U.P., Gupta, R.S., Kapur, V.K. On the steady performance of annular hydrostatic thrust bearing: Rabinowitsch fluid model. *J Tribol-T ASME* 134 044502 (2012) **DOI:10.1115/1.4007350**.

[8] Gustafsson, T., Rajagopal, K.R., Stenberg, R., Videman, J. Nonlinear Reynolds equation for hydrodynamic lubrication. *Appl Math Model* 39 5299-5309 (2015) **DOI:10.1016/j.apm.2015.03.028**.

[9] Yang, Q, Huang, P, Fang, Y A novel Reynolds equation of non-Newtonian fluid for lubrication simulation. *Tribol Int* 94 458-463 (2016) **DOI:10.1016/j.triboint.2015.10.011**.

[10] Masjedi, M., Khonsari, M.M. On the effect of surface roughness in point-contact EHL: Formulas for film thickness and asperity load. *Tribol Int* 82 228-244 (2015) **DOI:10.1016/j.triboint.2014.09.010**.

[11] El Khlifi, M., Souchet, D., Hajjam, M., Bouyahia, F. Numerical modeling of non-Newtonian fluids in slider bearings and channel thermohydrodynamic flow. *J Tribol-T ASME* 129 695-699 (2007) **DOI:10.1115/1.2736732**.

[12] Li, J., Chen, H. Evaluation on applicability of Reynolds equation for squared transverse roughness compared to CFD. *J Tribol-T ASME* 129 963-967 (2007) **DOI:10.1115/1.2768619**.

[13] Liu, Z., Wang, Y., Cai, L., Cheng, Q., Zhang, H. Design and manufacturing model of customized hydrostatic bearing system based on cloud and big data technology. *Int J Adv Manuf Tech* 84 261-273 (2016) **DOI:10.1007/s00170-015-8066-2**.

[14] Khakse, P., Phalle, V., Mantha, S. Performance analysis of a nonrecessed hybrid conical journal bearing compensated with capillary restrictors. *J Tribol-T ASME* 138 011703 (2016) **DOI:10.1115/1.4030808**.

[15] Kennedy, J., Eberhart, R. Particle swarm optimization. *IEEE International Conference on Neural Networks* 4 1942-1948 (1995) **DOI:10.1109/ICNN.1995.488968**.

[16] Eberhart, R., Shi, Y. Comparing inertia weights and constriction factors in particle swarm optimization. *IEEE World Congress on Evolutionary Computation* 1 84-88 (2000) **DOI:10.1109/CEC.2000.870279**.

[17] Schutte, J.F., Koh, B., Reinbolt, J.A., Haftka, R.T., George, A.D., Fregly, B.J. Evaluation of a particle swarm algorithm for biomechanical optimization. *ASME J Biomech Eng* 127 465-474 (2005) **DOI:10.1115/1.1894388**.

[18] Khajehzadeh, M., El-Shafie, A., Raihan, T. Modified particle swarm optimization for probabilistic slope stability analysis. *Int J Phys Sci* 5 2248-2258 (2010).

[19] Yan, Z., Deng, C., Zhou, J., Chi, D. A novel two subpopulation particle swarm optimization. *IEEE World Congress on Intelligent Control and Automation* 4113-4117 (2012) **DOI:10.1109/WCICA.2012.6359164**.

[20] Niu, P., Cheng, Q., Zhang, T., Yang, C., Zhang, Z., Liu, Z. Hyperstatic mechanics analysis of guideway assembly and motion errors prediction method under thread friction coefficient uncertainties. *Tribol Int* 108275 (2023) **DOI:10.1016/j.triboint.2023.108275**.

[21] Chen, H., Li, S. Multi-sensor fusion by CWT-PARAFAC-IPSO-SVM for intelligent mechanical fault diagnosis. *Sensors* 3647 (2022) **DOI:10.3390/s22103647**.

[22] Zhou, J., Wu, S.-S., Liu, T., Wu, X. Application of IPSO-MCKD-IVMD-CAF in the compound fault diagnosis of rolling bearing. *Meas Sci Technol* 34 035113 (2023) **DOI:10.1088/1361-6501/aca349**.

[23] Paikray, H.K., Das, P.K, Panda, S. Optimal multi-robot path planning using particle swarm optimization algorithm improved by sine and cosine algorithms. *Arab J Sci Eng* 46 3357-3381 (2021) **DOI:10.1007/s13369-020-05046-9**.

[24] Zhang, Q., Chen, S., Fan, Z.P. Bearing fault diagnosis based on improved particle swarm optimized VMD and SVM models. *Adv Mech Eng* 13 (2021) **DOI:10.1177/16878140211028451**.

[25] Sana, M.U., Li, Z., Javaid, F., Hanif, M.W., Ashraf, I. Improved particle swarm optimization based on blockchain mechanism for flexible job shop problem. *Cluster Comput* 26 2519-2537 (2023) **DOI:10.1007/s10586-021-03349-6**.

[26] Liu, K., Wu, S., Luo, Z., Gongze, Z., Ma, X., Cao, Z., Li, H. An intelligent fault diagnosis method for transformer based on IPSO-gcForest. *Math Probl Eng* 6610338 (2021) **DOI:10.1155/2021/6610338**.

[27] Cheng, Q., Zhan, C., Liu, Z., Zhao, Y., Gu, P. Sensitivity based multidisciplinary optimal design of a hydrostatic rotary table with particle swarm optimization. *Stroj Vestn-J Mech E* 61 432-447 (2015) **DOI:10.5545/sv-jme.2015.2478**.

[28] Chang, S.H., Jeng, Y.R. A modified particle swarm optimization algorithm for the design of a double pad aerostatic bearing with a pocketed orifice-type restrictor. *J Tribol-T ASME* 136 021701 (2013) **DOI:10.1115/1.4026061**.

[29] Srisha Rao, M.V., Jagadeesh, G. Vector evaluated particle swarm optimization (VEPSO) of supersonic ejector for hydrogen fuel cells. *J Fuel Cell Sci Tech* 7 041014 (2010) **DOI:10.1115/1.4000676**.

[30] Tang, D., Dai, M., Salido, M., Giret, A. Energy efficient dynamic scheduling for a flexible flow shop using an improved particle swarm optimization. *Comput Ind* 81 82-95 (2016) **DOI:10.1016/j.compind.2015.10.001**.

[31] Luo, W., Sun, J., Bu, C., Liang, H. Species-based particle swarm optimizer enhanced by memory for dynamic optimization. *Appl Soft Comput* 47 130-140 (2016) **DOI:10.1016/j.asoc.2016.05.032**.

[32] Liu, Z., Wang, Y., Cai, L., Zhao, Y., Cheng, Q., Dong, X. A review of hydrostatic bearing system: Researches and applications. *Adv Mech Eng* 9 (2017) **DOI:10.1177/1687814017730536**.

[33] Clerc, M., Kennedy, J. The particle swarm-explosion, stability, and convergence in a multidimensional complex space. *IEEE Trans Evolut Comp* 6 58-73 (2002) **DOI:10.1109/4235.985692**.

[34] Michalec, M., Svoboda, P., Křupka, I., Hartl, M. A review of the design and optimization of large-scale hydrostatic bearing systems. *Eng Sci Technol* 24 936-958 (2021) **DOI:10.1016/j.jestch.2021.01.010**.

[35] Li, X., Cheng, T., Li, M., Li, M., Wu, R., Wan, Y. Theoretical research on sector oil-pads mechanical property in hydrostatic thrust bearing based on constant flow. *Ind Lubr Tribol* 69 491-506 (2017) **DOI:10.1108/ILT-03-2016-0060**.

[36] Wang, Y., Liu, Z., Cai, L., Cheng, Q., Dong, X. Optimization of oil pads on a hydrostatic turntable for supporting energy conservation based on particle swarm optimization. *J Mech Eng* 64 95-104 (2018) **DOI:10.3901/JME.2018.22.095**.

[37] Cai, L., Wang, Y., Liu, Z., Cheng, Q. Carrying capacity analysis and optimizing of hydrostatic slider bearings under inertial force and vibration impact using FDM. *J Vibroeng* 17 2781-2794 (2015).

[38] Weißbacher, C., Schellnegger, C., John, A., Buchgraber, T., Pscheidt, W. Optimization of journal bearing profiles with respect to stiffness and load-carrying capacity. *J Tribol-T ASME* 136 031709 (2014) **DOI:10.1115/1.4027399**.

[39] Eberhart, R., Shi, Y. Comparing inertia weights and constriction factors in particle swarm optimization. *IEEE World Congress on Evolutionary Computation* 1 84-88 (2000) **DOI:10.1109/CEC.2000.870279**.

Acknowledgement *This research was supported by the National Natural Science Foundation of China (52075012).*

Data availability *The data that support the findings of this study are available from the corresponding author upon reasonable request.*

Received: 2025-04-23, revised: 2025-10-16, accepted: 2025-11-17 *as Original Scientific Paper.*

Author contributions *All authors contributed to the conceptualization and design of the study and participated in extensive revisions and approved the final version. Jiaqing Luo: Writing – original draft, Software, Formal analysis, Data curation; Yongsheng Zhao Data curation, Validation, Writing – review & editing; Ying Li: Writing – review & editing; Tao Zhang: Writing – review & editing; Honglie Ma: Writing – review & editing*

Declarations *The author declares that there are no competing interests.*

Metoda za optimalno načrtovanje hidrostatične vrtljive mize na osnovi FPSO algoritma

Povzetek *Nosilnost hidrostatičnih vrtljivih miz je v veliki meri odvisna od zasnove oljnih blazinic. Optimizacija parametrov oljnih blazinic lahko bistveno izboljša zmogljivost vrtljive mize ter hkrati zmanjša porabo energije. V tej študiji je predstavljen algoritem mehke optimizacije z rojem delcev (FPSO), ki v osnovno optimizacijo z rojem delcev (PSO) vpeljuje faktorje stisljivosti za optimizacijo parametrov oljnih blazinic. Rezultati optimizacije kažejo, da je rabo energije je mogoče zmanjšati za približno 40 %. Rezultati so bili potrjeni tudi eksperimentalno, pri čemer je razlika med eksperimentalnimi in teoretičnimi vrednostmi le 8 %. V primerjavi s tradicionalnimi PSO-algoritmi, FPSO kaže zanesljivejšo konvergenco pri večparametričnih problemih.*

Ključne besede *hidrostatična vrtljiva miza, metoda končnih razlik, Reynoldsova enačba, algoritem mehke optimizacije z rojem delcev, zmogljivost optimizacije*